Editors' Suggestion

Stability study of intense hadron bunches in linear accelerators using a Paul ion trap

M. Goto, C. Ichikawa, K. Ito, K. Kojima, and H. Okamoto*

Graduate School of Advanced Science and Engineering, Hiroshima University, 1-3-1 Kagamiyama, Higashi-Hiroshima 739-8530, Japan

(Received 3 February 2022; accepted 18 April 2022; published 5 May 2022)

The collective behavior of an ion cloud confined in a linear Paul trap is physically almost equivalent to that of a relativistic beam traveling in a particle accelerator. This fact provides a new possibility for experimental beam-dynamics studies that can be done without relying on large-scale machines. We have constructed a compact ion trap to explore various accelerator-physics issues in a local tabletop environment. The present trap system is designed particularly for the study of high-intensity short hadron bunches typical in linear accelerators. Resonance-induced ion losses are measured and plotted as a function of the betatron and synchrotron phase advances over a wide range, which offers a piece of indisputable experimental evidence for the presence of various betatron and synchrobetatron resonance stop bands. We confirm that these instability bands shift in the stability map depending on the ion density. The recently proposed stop-band diagram, free from the conventional concept of incoherent tune spread, is employed to explain the experimental observations.

DOI: 10.1103/PhysRevAccelBeams.25.054201

I. INTRODUCTION

Detailed information about space-charge effects in intense hadron beams is vital to design next-generation accelerators as well as to improve the performance of existing high-intensity machines. The recent progress of accelerator technology has made it feasible to confine a huge number of charged particles in a tiny configuration space. The motions of individual particles forming a dense beam core are then no longer independent but rather strongly correlated due to the long-range nature of Coulomb interaction [1,2]. The systematic study of such collective beam behavior is extremely difficult to conduct. It is necessary to solve the complicated equations of motion of interacting particles in a self-consistent manner, which seems almost hopeless to achieve mathematically. The use of numerical simulation techniques is an alternative powerful approach, but high-precision three-dimensional (3D) computation requires very long CPU time even with modern workstations. Various practical problems are also encountered in experiments as long as we rely on large-scale accelerators. The flexibility and controllability of fundamental parameters are quite limited in accelerator-based experiments. For instance, it is difficult to perform a full-range survey of the betatron and synchrotron tune space. Note also that any operating machine consisting of many components inevitably includes mechanical errors and noise sources that complicate the beam motion.

These practical difficulties in conventional approaches motivated us to develop an entirely new experimental system called "S-POD" (Simulator of Particle Orbit Dynamics) [3]. The S-POD is based on the physical similarity between a relativistic charged-particle beam focused by an alternating-gradient (AG) quadrupole lattice and a non-neutral plasma stored in a linear Paul trap (LPT) [4,5]. These two multiparticle dynamical systems are governed by the same closed set of equations of motion. This means that in the compact LPT, we can reproduce the space-charge-induced phenomena equivalent to those expected in a large-scale accelerator.

There are four independent S-POD systems currently operational at the Beam Physics Laboratory of Hiroshima University. Three of them were constructed to elucidate the transverse beam stability. Long ion clouds of a sausage-like configuration are produced there by a nearly square-well potential along the LPT axis. The effect of synchrobetatron coupling is then negligible, which allows us to concentrate upon betatron stability issues. A lot of information about the fundamentals of transverse space-charge effects have been accumulated through a decade of experimental effort [6–14]. We are now ready to move forward to extend our research incorporating longitudinal effects. The stability of the synchrotron motion together with the betatron motion is explored experimentally in the present work using

*Corresponding author.
okamoto@sci.hiroshima-u.ac.jp

high-density short ion clouds. The fourth S-POD constructed recently is intended for this purpose.

The synchrotron tune is generally very low in circular accelerators where the bunch length is far greater than the transverse beam size. In contrast, the bunch shape is ellipsoidal or even spherical in linear accelerators because of comparable tunes in the three spatial directions [15,16]. The interplay between the betatron and synchrotron motions could then give rise to additional undesired effects on beam stability. Furthermore, the interparticle Coulomb interaction is more severe in linear machines as they are employed in a low beam-energy region. Understanding space-charge effects in a short bunch is thus especially important to establish a reliable guideline for the design of high-intensity hadron linacs. The new S-POD system mentioned above can produce a high-density ion cloud with the aspect ratio of around unity, enabling us to explore space-charge issues in linacs.

In Sec. II, we start with an overview of the LPT structure and typical experiment conditions. Some structural parameters of essential importance in evaluating accurate tunes are determined in Sec. III from S-POD outputs at low ion density. We then proceed to high-intensity measurement results in Sec. IV. After examining the maximum number of ions confineable in the present LPT and the lifetime of a stored ion cloud, we show the stability tune diagrams obtained with the S-POD at different bunch intensities and ion confinement periods. Finally, a brief summary is given in Sec. V.

II. S-POD FOR SHORT-BUNCH EXPERIMENT

A typical LPT is composed of four electrode rods symmetrically placed around the trap axis [17]. The radio-frequency (rf) voltages $\pm V_\perp$ are applied to these rods, as illustrated in Fig. 1, to generate an electric quadrupole field for transverse ion confinement. The dedicated LPT for short-bunch experiment is axially divided into three electrically isolated quadrupole sections. The aperture radius r_0, i.e., the minimum distance from the LPT axis to the rod surfaces, is 5 mm. The radius ρ of each rod is chosen to be 5.75 mm at which the nonlinearity of the aperture field is minimized. An axial potential well is created by adding an identical bias voltage $U_\parallel$ to the two quadrupole sections on both sides of the central section where ions are stored. The number of ions surviving after a certain storage period is measured with a microchannel plate (MCP) detector. The length of the central electrodes is 8.9 mm, which has been optimized to form an approximately parabolic potential well by $U_\parallel$ [18]. Although $U_\parallel$ is generally time-dependent, we have made it static for the sake of simplicity. The synchrotron resonance is, therefore, not directly excited in the present study.

Consider an LPT that confines ions of rest mass M and charge state q at the rf frequency $f_{\rm rf}$. The ion cloud stored in the LPT obeys the following Hamiltonian, provided that

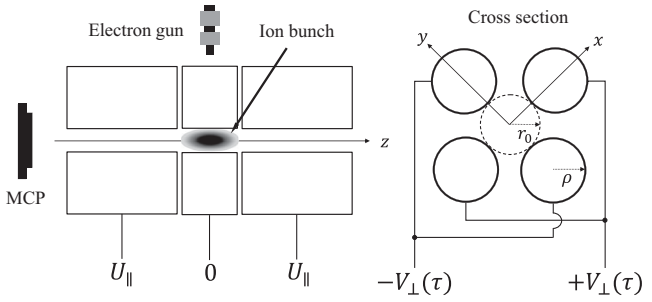

FIG. 1. Schematic drawing of the LPT for short-bunch experiment. The LPT consists of three quadrupole sections electrically isolated from each other. The transverse rf quadrupole field of the same strength is always excited in all three sections. The central section, in which ions are stored, is 8.9 mm long; this length is determined so as to make the axial potential well nearly parabolic when an equal DC bias voltage is applied to the two end sections of 30 mm long. An electron gun is placed above the central section to ionize neutral Ar atoms. The radii of the aperture and quadrupole rods are $r_0 = 5$ mm and $\rho = 5.75$ mm. The DC bias $U_\parallel$ on the MCP side is dropped to extract remaining ions and count them with the detector.

the axial potential generated by $U_\parallel$ is approximately quadratic [18]:

$$H = \frac{1}{2}\left[p_r^2 + \left(\frac{p_\theta}{r}\right)^2 + p_z^2\right] + \left[\frac{qV_\perp(\tau)}{Mc^2}\left(\frac{L}{r_0}\right)^2 \cos 2\theta - \frac{\sigma_{0\parallel}^2}{4}\right]\left(\frac{r}{L}\right)^2 + \frac{\sigma_{0\parallel}^2}{2}\left(\frac{z}{L}\right)^2 + \frac{q}{Mc^2}\phi_{\rm sc}, \quad (1)$$

where (p_r, p_θ, p_z) are the canonical momenta conjugate to the cylindrical coordinates (r, θ, z), the independent variable is $\tau = ct$ with c and t being the speed of light and time, $\phi_{\rm sc}$ is the Coulomb self-field potential satisfying the Poisson equation, and $L \equiv c/f_{\rm rf}$. This Hamiltonian has the same form as the one often assumed in standard space-charge theories to describe the hadron beam behavior in linear accelerators [1,19–22]. The parameter $\sigma_{0\parallel}$ in Eq. (1) is defined by $\sigma_{0\parallel}^2 = 2(L/\ell_z)^2(qU_\parallel/Mc^2)$ that corresponds to the synchrotron phase advance per unit AG cell when $U_\parallel$ is constant. ℓ_z is the characteristic length of the plasma confinement region depending on the mechanical design of the LPT; it is generally a bit shorter than the central rod length. A numerical analysis with a 3D Maxwell-equation solver concludes that $\ell_z \approx 8.23$ mm for the LPT structure in Fig. 1.

The ion species used for the S-POD experiment has nothing to do with the essence of the physical process we are interested in; the mass and charge state of the ions are simply scaling parameters. We adopted $^{40}Ar^+$ ions that can be produced easily from neutral Ar gas atoms through the

electron bombardment process. The nominal operating rf frequency of the LPT is set at 1 MHz. Ideally, the rf waveform of $V_\perp$ is adjusted to reflect the discrete AG focusing lattice of a particular linac, in other words, the spatial arrangement of quadrupole magnets along the beam line. The most popular AG structure is the so-called FODO (focus-drift-defocus-drift) lattice [23].

Instead of a pulse waveform, we here take the simple sinusoidal focusing potential to model the FODO lattice; namely, $V_\perp(\tau) = V_{\rm rf}\cos(2\pi\tau/L)$ with $V_{\rm rf}$ being a constant rf amplitude. It is known that the sinusoidal lattice has a resonance feature very similar to the FODO lattice [12,22]. For $^{40}Ar^+$ ions, the rf voltage $V_{\rm rf}$ necessary to achieve a large betatron phase advance of 144° (the bare tune of 0.4) per cell is only about 88.9 V at the operating frequency of 1 MHz if the transverse defocusing effect from the axial focusing potential is negligible. In a short bunch, however, this defocusing effect on the betatron motion is rather strong. The rf amplitude must be increased from 88.9 V to 100.5 V in the above case when the synchrotron phase advance is adjusted to 90° per cell, for example.

III. CALIBRATION OF STRUCTURAL PARAMETERS

The conditions of space-charge-induced instabilities are well characterized by a few physical quantities, namely, the beam density in phase space and the three bare tunes per unit focusing cell. The convenient measure of the phase-space density is the root-mean-squared (rms) *tune depression* η that ranges from 0 to 1. $\eta \approx 1$ at low density where the effective tune is close to the design value with no space-charge-induced shift. η is reduced as the density becomes higher or, in other words, the beam temperature becomes lower. At the absolute zero temperature where $\eta = 0$, the beam is Coulomb crystallized [24]. Multiplying the bare tunes by 2π, we have the bare phase advances $(\mu_{0x}, \mu_{0y}, \sigma_{0\|})$ commonly used in the linac community. Since the horizontal and vertical betatron phase advances in typical linacs are close, we assume $\mu_{0x} = \mu_{0y}(\equiv\mu_{0\perp})$ throughout the present experimental study.

The synchrotron phase advance $\sigma_{0\|}$ is determined solely by the axial focusing potential provided by the bias $U_\|$. On the other hand, the betatron phase advance $\mu_{0\perp}$ depends not only on the rf quadrupole amplitude $V_{\rm rf}$ for transverse focusing but also on $U_\|$ as is evident from Eq. (1). As remarked above, the bias voltage $U_\|$ added to the two end sections for axial ion confinement inevitably yields a transverse defocusing force. This corresponds directly to the effect known as *rf defocusing* in accelerating gaps [23].

In the S-POD experiment, the bare phase advances can be calculated from the waveform and amplitude of the voltages applied to the electrodes if all the other parameters in Eq. (1) are known. $V_{\rm rf}$ and $U_\|$ supplied by our power sources are monitored in every measurement to derive the actual phase advances as precisely as possible. The effective magnitudes of r_0 and ℓ_z in the Hamiltonian may, however, be slightly different from the ideal design values due to mechanical errors. It is thus required to figure out their real values somehow for accurate determination of the three phase advances. For the calibration of these structural parameters, we paid attention to the tune dependence of ion losses caused by some low-order resonances.

Similarly to any particle accelerators, the external ion-focusing potential in the LPT is not perfectly linear as assumed in Eq. (1). The electric field in the LPT aperture includes weak nonlinear components induced by mechanical errors. Those nonlinearities give rise to resonant ion losses that can be enhanced easily by extending the ion storage period. At low ion density where the effect of interparticle Coulomb interaction is negligible, we expect ion losses to occur under the *single-particle resonance* condition

$$n_\perp\mu_{0\perp} + n_\|\sigma_{0\|} = 2\pi n, \tag{2}$$

where $n_\perp$, $n_\|$, and n are integers [25,26]. For the determination of the effective r_0 and ℓ_z, we used the loss signals from the three relatively strong resonances with $(n_\perp, n_\|, n) = (3,0,1)$, (4,0,1), and (2,2,1) identified in preliminary measurements.

The space-charge-induced shift of the phase advances must be minimized to improve the calibration accuracy. We confirmed that the shift can be made negligible by reducing the initial ion number $N_{\rm in}$ well below 10^4. $N_{\rm in}$ was, therefore, chosen to be about 10^3 in the calibration experiment. The number of surviving ions after 1 s, corresponding to beam transport over a million AG cells, was measured with the MCP to locate the positions of the above-mentioned three nonlinear resonances with $U_\|$ fixed at 3.14 V, 10.89 V, 18.00 V, and 22.09 V. These four bias voltages give the synchrotron phase advances $\sigma_\| = 27.1°$, 50.6°, 64.8°, and 72.0°, respectively, if the effective r_0 and ℓ_z agree with the ideal theoretical values, i.e., $r_0 = 5.00$ mm and $\ell_z = 8.23$ mm. We varied $\mu_{0\perp}$ over a wide range to search for the resonances while keeping $U_\|$.

The measurement results in the two cases where $U_\| = 3.14$ V and 10.89 V are exhibited in Fig. 2. Three vertical lines in each panel are the theoretically expected positions of the resonances with $(n_\perp, n_\|, n) = (3,0,1)$, (4,0,1), and (2,2,1). Under the condition that $r_0 = 5.00$ mm and $\ell_z = 8.23$ mm, these lines are slightly deviated from the actual loss positions as seen in Fig. 2(a). A similar small discrepancy between the theoretical expectation and experimental observation is also found in the other two cases where $U_\| = 18.00$ V and 22.09 V. We applied the least-squares method to minimize the discrepancies in all four cases simultaneously, using r_0 and ℓ_z as free parameters. After the calibration, the ion-loss positions move exactly on

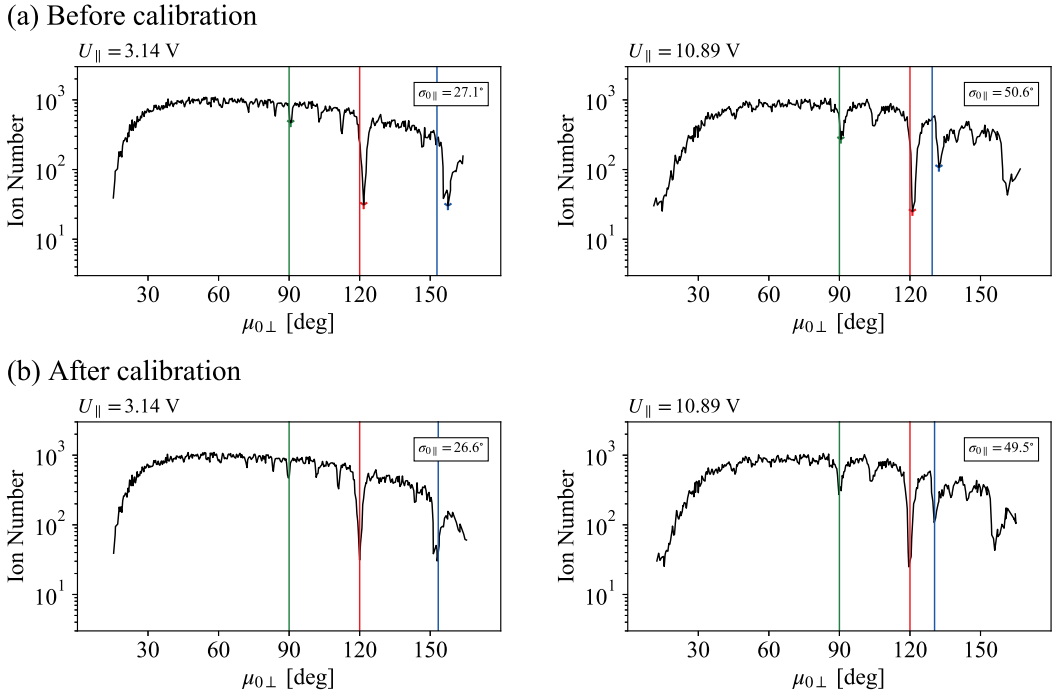

FIG. 2. Long-term ion-loss distribution in the low-density regime. The number of Ar^+ ions remaining in the LPT after 1 s (10^6 sinusoidal periods) is measured at many different values of $\mu_{0\perp}$ with the axial confinement bias fixed at $U_\parallel = 3.14$ V and $U_\parallel = 10.89$ V. Each curve consists of 360 data points. Three vertical lines indicate the locations of the resonances expected from Eq. (2) with $(n_\perp, n_\parallel, n) = (3, 0, 1)$ (red), (4,0,1) (green), and (2,2,1) (blue). The ideal structural parameters, i.e., $r_0 = 5.00$ mm and $\ell_z = 8.23$ mm, are assumed in the upper panels (a) to determine the bare phase advances. In the lower panels (b), these parameters are modified to $r_0 = 5.022$ mm and $\ell_z = 8.397$ mm. In addition to the three resonances above, we notice several other resonances that should be of the fourth and fifth orders according to Eq. (2). For instance, the cause of the two small dips between the green and red lines in the left panels can be understood as the nonlinear resonances with $(n_\perp, n_\parallel, n) = (3, 2, 1)$ and (3,1,1). These high-order resonances have only little impact on bunch stability in a short timescale corresponding to the length of a typical hadron linac, unless they are driven by strong error fields.

the vertical line as shown in Fig. 2(b) where r_0 and ℓ_z are corrected to 5.022 mm and 8.397 mm, respectively. We repeated the same experimental procedure several times to check the reproducibility and concluded that $r_0 = 5.024 \pm 0.002$ mm and $\ell_z = 8.370 \pm 0.040$ mm.

IV. EXPERIMENTAL RESULTS

A. LPT performance test

Before constructing stability tune diagrams at various bunch intensities, we tested the basic LPT performance. One of the important pieces of information is the long-term acceptance of the LPT with fixed operating phase advances. In typical S-POD experiments, we first generate an ion cloud of a certain intensity at a proper operating point where the ion stability is guaranteed. The operating point is then quickly moved to any target point to see whether the bunch is stable there for a specific storage period. This procedure allows us to start each stability measurement with nearly the same ion cloud, as if we inject an ion beam of particular intensity and emittance into a linac independently of the operating phase advances.

We usually spend 100 μs (100 AG cells) to move the operating point to a target position. This gradual change in the external focusing force causes no serious mismatch in the particle distribution and thus almost no additional losses. It is of course possible to make the sweep speed much slower if necessary, but that results in non-negligible extra particle losses due to the resonance crossing mentioned later. A question now is what tunes we should choose for the preparation of an initial ion bunch. Since the ionization process lasts typically for a million AG periods, a poor choice of the betatron and synchrotron phase advances makes it impossible to provide a bunch of sufficient intensity.

The number of surviving ions after the long ionization process was measured at 6000 different operating points. The result is color-coded in Fig. 3 revealing the existence of several strong resonance bands. It turns out that the acceptance of the dynamical system governed by the approximate Hamiltonian in Eq. (1) is significantly improved in a low tune range where $\mu_{0\perp} \lesssim 60°$ and $\sigma_{0\parallel} \lesssim 30°$. The maximum number of confineable ions was about 3.8×10^6 achieved around $(\mu_{0\perp}, \sigma_{0\parallel}) = (50.0°, 26.4°)$. This optimum operating

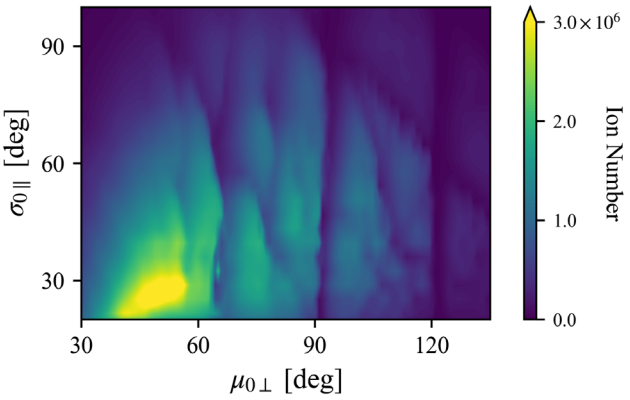

FIG. 3. Number of confineable ions with the betatron and synchrotron phase advances fixed through the whole experiment process from the ion production to the extraction. The map contains 6000 independent data points. The final ion number at each operating point was measured after the routine ionization procedure of 1 s long, followed by 51.2-ms storage.

point is always used in the following experiments for the production of an ion bunch.

The next question is how fast an ion cloud naturally decays due to collisions with residual gas atoms as well as Coulomb scattering. Figure 4 shows the time evolution of the surviving ion number when the operating point is fixed at $(\mu_{0\perp}, \sigma_{0\parallel}) = (50.0°, 26.4°)$. Three different bunch intensities are considered in the picture. In each case, we repeated the same measurement procedure five times and took the average to determine the positions of markers. The reproducibility is very good as is evident from the sizes of error bars. We recognize that all three cases have two characteristic decay constants, which is typical in regular LPTs [13,27]. The ion number $N(t)$ remaining in the LPT at time t can be fitted fairly well with the two-component exponential function

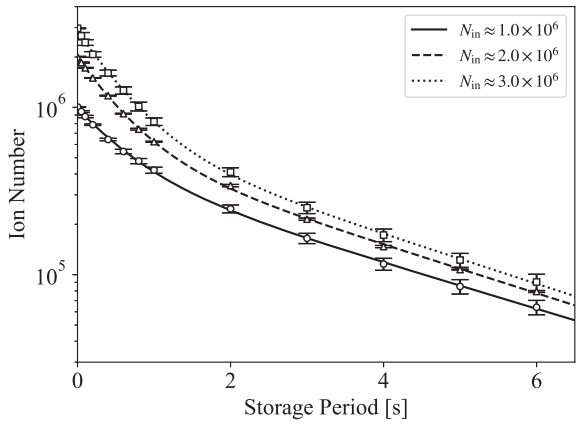

FIG. 4. Long-term decay of stored ions at the operating point $(\mu_{0\perp}, \sigma_{0\parallel}) = (50.0°, 26.4°)$. The initial ion number N_{in} is adjusted to about 1×10^6 (solid), 2×10^6 (dashed), and 3×10^6 (dotted). The three curves are obtained from the fitting function in Eq. (3) with the decay constants listed in Table I.

TABLE I. Decay constants measured at $(\mu_{0\perp}, \sigma_{0\parallel}) = (50.0°, 26.4°)$.

Initial ion number $N(0)$	$\sim 1 \times 10^6$	$\sim 2 \times 10^6$	$\sim 3 \times 10^6$
T_S [s]	0.60	0.53	0.53
T_L [s]	3.16	2.99	2.93

$$N(t) = N_S \exp\left(-\frac{t}{T_S}\right) + N_L \exp\left(-\frac{t}{T_L}\right), \quad (3)$$

where N_S and N_L are constant coefficients. T_S and T_L represent the e-folding lifetimes corresponding, respectively, to the relatively rapid decay in an early stage and to the slow decay after the storage period of around 1 s.

The fitting results are summarized in Table I. T_L is around 3 s even at such high ion density. From a practical point of view, T_S is more important because most hadron linacs consist of a limited number of AG focusing cells. For instance, the Alvarez-type drift-tube linac (DTL) at the Japan Proton Accelerator Research Complex includes only less than a hundred FODO cells [16]. Storing ions in the LPT for 0.1 ms is thus sufficient to simulate the proton-beam behavior in this linac, while the e-folding lifetime in the early stage is over 500 ms at the ionization point. The beam stability diagrams shall be constructed in the next subsection with the S-POD data obtained for ion-storage periods of shorter than 10 ms at most. T_S tends to be shortened in a higher-tune region but still much longer than 10 ms unless the operating point is in a resonance band. Natural ion losses due to interparticle collisions can, therefore, be ignored in the present experimental study of high-intensity linacs.

The axial potential barrier created by the DC bias $U_\parallel$ on the MCP side is removed after a specific storage period to measure the number of surviving ions. In this ion extraction process, we must be careful about the effect from the sudden removal of the axial confinement potential. When ions are stored at an operating point with a large $\sigma_{0\parallel}$, the disappearance of the transverse rf defocusing term enhances $\mu_{0\perp}$ considerably, leading to possible instability of the betatron motion. Such transverse overfocusing actually takes place as demonstrated in Fig. 5. In this experiment, we first accumulated roughly 2×10^6 ions at $(\mu_{0\perp}, \sigma_{0\parallel}) = (50.0°, 26.4°)$ and then changed both phase advances almost linearly within 100 μs to target values.

Each curve in Fig. 5 corresponds to the case where the synchrotron phase advance $\sigma_{0\parallel}$ right before the removal of the axial potential barrier is set at $\sigma_{0\parallel} = 26.4°$ (solid) or 70.7° (dashed) or 88.3° (dotted). In all cases, the operating point is maintained for 150 μs after arriving at the target location in the $\mu_{0\perp}$-$\sigma_{0\parallel}$ plane. A rapid drop of the output ion signal at the MCP was observed, depending on $\sigma_{0\parallel}$ before the extraction. The stability threshold of ion transport was lowered at a higher $\sigma_{0\parallel}$ as expected.

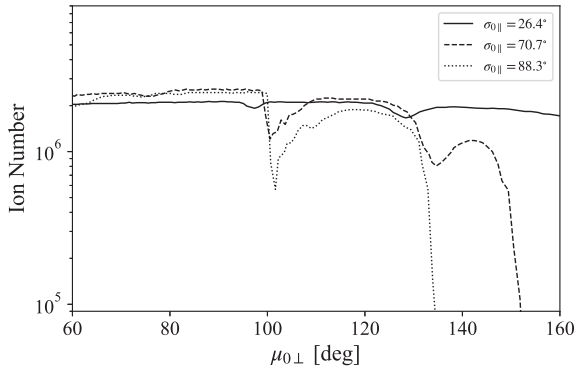

FIG. 5. Ion losses due to the transverse overfocusing effect caused by the removal of an axial potential barrier. The transverse phase advance $\mu_{0\perp}$ is varied over a wide range with the synchrotron phase advance adjusted to $\sigma_{0\parallel} = 26.4°$, 70.7°, and 88.3°. An ion bunch is generated initially at $(\mu_{0\perp}, \sigma_{0\parallel}) = (50.0°, 26.4°)$ in all three cases. After about 2×10^6 ions are accumulated there, the operating point is quickly moved onto a fixed-$\sigma_{0\parallel}$ line and stay there for 150 μs before ion extraction.

To avoid this strong instability irrelevant to the resonance phenomenon, we simply returned the operating point back to the original location, i.e., $(\mu_{0\perp}, \sigma_{0\parallel}) = (50.0°, 26.4°)$, spending another 100 μs. This procedure guarantees stable ion transport to the MCP. Note, however, that the operating point may cross one or more resonance bands when the target operating point is far from the ionization point. The effect of resonance crossing is probably not so serious at such high crossing speed [7], but some small extra ion losses will be unavoidable, depending on the strength of the resonance crossed.

B. Stability maps

About 6000 independent measurements were carried out at 6000 different combinations of $(\mu_{0\perp}, \sigma_{0\parallel})$ distributed uniformly in the tune space. The number of ions surviving after a specific storage period is color-coded in Figs. 6 and 7 over the ranges $20° \le \mu_{0\perp} \le 160°$ and $20° \le \sigma_{0\parallel} \le 100°$. The ion-storage period at each operating point is fixed in Fig. 6 at 0.5 ms corresponding to beam transport over 500 AG cells. It is extended to 10 ms in Fig. 7 to enhance ion losses for identification of weak nonlinear resonances. Many instability bands have appeared, indicating the presence of not only noncoupling betatron resonances but also sum and difference resonances among the three spatial degrees of freedom. All resonance bands have been considerably shifted from the solid and dashed lines drawn on the basis of the single-particle resonance condition in Eq. (2). The band shifts are quite large and dependent on the initial bunch intensity. Significant ion losses near the upper left corner of the diagrams have nothing to do with resonances. The primary cause is the enhancement of nonlinear defocusing fields at high $U_{\parallel}$, resulting in the shrinkage of the LPT acceptance especially in the low $\mu_{0\perp}$ range where the transverse focusing is relatively weak.

We find that the stop bands are not in parallel with the single-particle resonance lines. As explained in the last subsection, an ion bunch of certain intensity is produced at $(\mu_{0\perp}, \sigma_{0\parallel}) = (50.0°, 26.4°)$ before moving to a target operating point for stability measurement. The bunch is more strongly compressed when the target phase advances are higher than the values at the initial ionization point. As a result, the shift of a stop band from the neighboring single-particle resonance line tends to increase in a region of larger phase advances. The same tendency can be seen in the coherent stop-band diagram constructed theoretically in the Appendix.

We also recognize slight tune-independent ion losses everywhere in the region above the strong linear betatron resonance band ($\mu_{0\perp} > 90°$). The loss rate is clearly higher for a bunch of higher initial intensity. These extra ion losses detected even in resonance-free areas should be largely due to the effect of resonance crossing. The *coherent resonance* located just above $\mu_{0\perp} = 90°$ is particularly strong at high bunch intensity, which causes serious ion losses as confirmed repeatedly in past S-POD experiments [6–9,12]. This collective resonance is of the second order and often referred to as the *envelope instability* [1,28–34]. Since the operating point is eventually returned to $(\mu_{0\perp}, \sigma_{0\parallel}) = (50.0°, 26.4°)$ before ion extraction, it crosses the linear resonance band twice. This is a possible cause of the observed enhancement of ion losses in the high-$\mu_{0\perp}$ range.

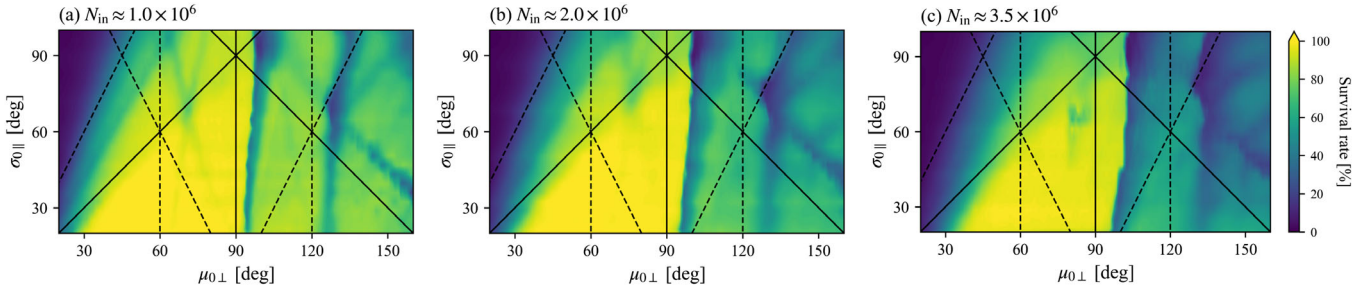

FIG. 6. Stability tune diagram for the ion storage period of 0.5 ms (500 AG cells). The number of ions confined initially in the LPT is adjusted to about (a) 1.0×10^6, (b) 2.0×10^6, and (c) 3.5×10^6.

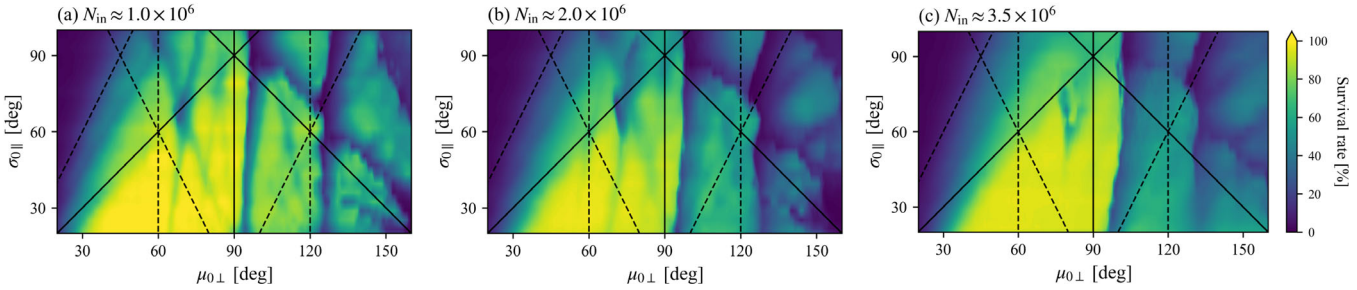

FIG. 7. Stability tune diagram for the ion storage period of 10 ms (10000 AG cells). The number of ions confined initially in the LPT is adjusted to about (a) 1.0×10^6, (b) 2.0×10^6, and (c) 3.5×10^6.

According to the single-particle resonance condition in Eq. (2) or *incoherent resonance* picture, the three solid lines in Figs. 6 and 7 are interpreted as fourth-order resonances. The resonances along the dashed lines are supposed to be of the sixth order, except for the one along $3\mu_{0\perp} = 360°$ that can be understood as the third order. The incoherent instability mechanism is, however, effective only in the *tail* (halo) part of the ion bunch as discussed in Refs. [35–37]. The tune shifts of individual particles forming the tail in six-dimensional phase space are relatively small in many cases because of the weak Coulomb coupling with the bunch *core* [38]. The observed shifts of the ion-loss bands seem too large to be attributed solely to the incoherent effect, implying that the coherent mechanism should be contributing to these losses.

The core resonance condition conjectured in Ref. [22] can be written as

$$n_\perp \mu_{0\perp}[1 - C_m(1 - \eta_\perp)] + n_\parallel \sigma_{0\parallel}[1 - C_m(1 - \eta_\parallel)] = \pi n', \tag{4}$$

where $\eta_\perp$ and $\eta_\parallel$ are the transverse and longitudinal rms tune depressions, n' is an integer, and C_m is the coherent tune-shift factor depending on the resonance order number m. Provided that the resonance driving term is proportional to $x^{|n_x|}y^{|n_y|}z^{|n_\parallel|}$ with n_x and n_y being integers, we have $m = |n_x| + |n_y| + |n_\parallel|$. C_m is slightly below unity (except for the dipole mode) [35,39,40]. As pointed out in the Appendix, this condition can roughly reproduce the instability regions observed in Figs. 6 and 7. Accepting the proposed coherent resonance theory, we only need the linear and lowest-order nonlinear resonances to cover all pronounced stop bands discovered in the experiment; the ion losses along the solid lines are due to the instability of the linear ($m = 2$) collective mode while those along the dashed lines to the instability of the third-order mode ($m = 3$). In addition to the envelope instability band with $(n_\perp, n_\parallel, n') = (2, 0, 1)$, another second-order resonance band with $(n_\perp, n_\parallel, n') = (1, 1, 1)$ is clearly visible. The role of this synchrobetatron sum resonance in a high-intensity linac design has been discussed theoretically in Ref. [41].

The pure synchrotron resonance with $n_\perp = 0$ will not be excited here because the axial confinement potential is static. Even if the bias voltage $U_\parallel$ varies periodically, no serious instability of the synchrotron motion is expected as long as a single FODO period includes two rf accelerating gaps [22]. In the typical case of Alvarez DTLs, a hadron bunch well-matched to the lattice executes an almost identical breathing oscillation twice longitudinally in every FODO cell, which suggests that the synchrotron phase advance per *effective* focusing period is a half of $\sigma_{0\parallel}$ defined here from the transverse lattice period. Synchrotron noncoupling resonances that may appear in the range $\sigma_{0\parallel} \lesssim 90°$ are then of the fourth order ($m = 4$) or higher and thus weak (unless driven by external error fields). We are now preparing for further S-POD experiment to verify what happens when $U_\parallel$ is periodic.

V. SUMMARY

A unique tabletop device called S-POD has been developed, which offers a multiparticle dynamical system physically equivalent to a hadron bunch in a quadrupole focusing lattice. The novel system enables us to acquire detailed experimental data useful for basic designs of next-generation high-intensity accelerators and also for the performance improvement of existing machines. Employing the S-POD, we surveyed a wide range of parameter space to identify the condition of resonant beam instability in which the Coulomb self-field potential plays an important role. The present study focuses on the stability of intense short bunches typical in injector linacs.

We succeeded in constructing the stability tune diagram that visualizes the distribution of resonance stop bands in the plane spanned by the transverse betatron phase advance $\mu_{0\perp}$ and the longitudinal synchrotron phase advance $\sigma_{0\parallel}$ per unit AG focusing cell. The excitation of betatron and synchrobetatron resonances was confirmed experimentally, depending on the bunch intensity.

A coherent resonance conjecture was introduced to explain the experimental results from the S-POD. According to the simple formula in Eq. (4), all observed ion-loss bands can naturally be interpreted as the consequences of the lowest ($m = 2$) and second lowest ($m = 3$)

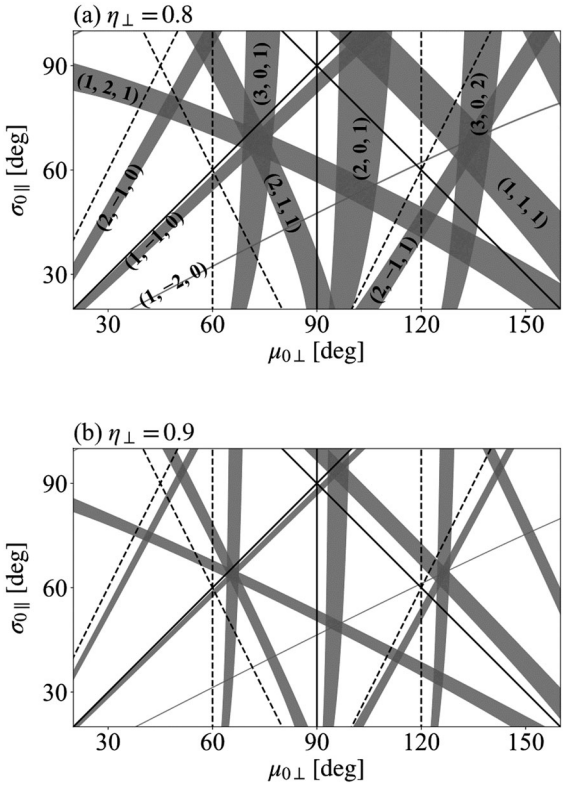

FIG. 8. Stability tune diagram obtained from the coherent resonance condition in Eq. (4) and the bandwidth formula in Eq. (A1). The coherent core instabilities of the second-order or third-order modes could be excited in gray shaded areas. The number of particles in a bunch is fixed everywhere at the value that corresponds to the two cases where (a) $\eta_\perp = 0.8$ and (b) $\eta_\perp = 0.9$ at the operating point $(\mu_{0\perp}, \sigma_{0\parallel}) = (50.0°, 26.4°)$. The bunch is assumed to be equipartitioned at this initial ionization point. Three numbers in the bracket written on each instability band represent $(n_\perp, n_\parallel, n')$ in Eq. (4) used to draw the band. The same solid and dashed lines as indicated in Figs. 6 and 7 are replotted for reference.

order resonances [42]. The large distance of each instability band from the corresponding single-particle resonance line suggests that the ion losses are caused mainly in the core region of the bunch, rather than in the tail region where the incoherent resonance of twice the order of the core resonance is expected to occur [35–37]. The stability map (Fig. 8) based on the coherent resonance condition in Eq. (4) together with the bandwidth formula in Eq. (A1) is in good qualitative agreement with the experimental observations.

APPENDIX: COHERENT STOP BANDS

Each coherent resonance of the beam core, predicted by Eq. (4), has a finite width depending on the beam density in phase space and even on the beam focusing lattice and particle distribution function. The bandwidth formula of a one-dimensional (1D) sheet beam has been derived mathematically in Ref. [40] taking the waterbag model. It is hopeless to obtain a similar analytic expression of the coherent bandwidth in multidimensional cases, but a concise formula applicable to coasting beams has been proposed in Ref. [37]. We generalize it for bunched beams to make a quick initial estimate of the approximate width $\delta w(n_\perp, n_\parallel)$ of a coherent stop band for arbitrary $n_\perp$ and $n_\parallel$. The most straightforward generalization should be the following:

$$\delta w(n_\perp, n_\parallel) = 2g(n_\perp, n_\parallel)(1 - C_m)\frac{1 - \bar{\eta}}{\bar{\eta}}\bar{\nu}_0, \quad \text{(A1)}$$

where $\bar{\eta} \equiv (\eta_\perp + \eta_\parallel)/2$, $\bar{\nu}_0 \equiv (\mu_{0\perp} + \sigma_{0\parallel})/2$, and

$$g(n_\perp, n_\parallel) \equiv \frac{|n_\parallel \varepsilon_\perp + n_\perp \varepsilon_\parallel|}{|n_\parallel|\varepsilon_\perp + |n_\perp|\varepsilon_\parallel} \quad \text{(A2)}$$

with $\varepsilon_{\perp(\parallel)}$ being the rms emittance in the transverse (longitudinal) direction. The factor $g(n_\perp, n_\parallel)$ reflects the fact that a difference resonance $(n_\perp n_\parallel < 0)$ of any order is strongly suppressed when $\Lambda(n_\perp, n_\parallel) \equiv \varepsilon_\perp/n_\perp + \varepsilon_\parallel/n_\parallel$ is close to zero [22]. Sacherer's Vlasov analysis for the 1D uniform beam predicts that $C_2 = 0.750$, $C_3 = 0.875$, and $C_4 = 0.922$ [39]. Similar numbers have been reached for the waterbag beam [40]. We here assume slightly different numbers concluded in a recent numerical study [35]; namely, $C_2 \approx 0.7$, $C_3 \approx 0.8$, and $C_4 \approx 0.9$.

Figure 8 shows the stability tune diagrams obtained from the proposed coherent resonance formulas. All core resonance bands associated with the linear $(m = 2)$ and first nonlinear $(m = 3)$ modes are drawn based on the core resonance condition in Eq. (4). The width of each instability band is estimated from Eq. (A1). Recalling the experimental condition for the production of an ion bunch in the LPT, we have fixed the bunch intensity everywhere in the diagram at the value that makes the transverse tune depression $\eta_\perp$ equal to 0.8 or 0.9 at the operating point $(\mu_{0\perp}, \sigma_{0\parallel}) = (50.0°, 26.4°)$. The longitudinal tune depression $\eta_\parallel$ is determined such that the bunch is in the equipartitioned state there [43]. The equipartitioning condition is broken at other operating points. It is informative to notice that the bandwidths are much narrower than the so-called *incoherent tune spread* of a Gaussian core.

The distribution of the low-order stop bands exhibited in Fig. 8 explains the experimental observations qualitatively. Most of the theoretically predicted stop bands can be seen in Figs. 6 and 7. Even the signatures of the third-order sum resonances with $(n_\perp, n_\parallel, n') = (1, 2, 1)$ and (2, 1, 2) are recognizable in a high-tune range $\mu_{0\perp} > 120°$ [see, e.g., Fig. 7(a)]. Note that the third-order stop band with $(n_\perp, n_\parallel, n') = (1, -2, 0)$ is extremely narrow under the condition assumed here. This difference resonance was actually unobservable in the experiment.

The comparison of the theoretical prediction in Fig. 8 with the S-POD data in Figs. 6 and 7 indicates that the tune depression at $(\mu_{0\perp}, \sigma_{0\parallel}) = (50.0°, 26.4°)$ may already exceed 0.9 with 1.0×10^6 ions in the LPT. $\eta_\perp$ is probably reduced to 0.8 or lower at $N_{\mathrm{in}} \approx 3.5 \times 10^6$ over a wide tune range. This is reasonable according to our past experience in long-bunch experiments where $\eta_\perp$ reached 0.8 with about 10^7 ions in another LPT whose quadrupole electrodes in the ion confinement section are roughly five times longer than the present design [44].

[1] See, e.g., M. Reiser, *Theory and Design of Charged Particle Beams* (John Wiley & Sons, New York, 2008) and references therein.

[2] See, e.g., *Proceeding of 54th ICFA Advanced Beam Dynamics Workshop on High-Intensity and High-Brightness Beams (HB2014), Michigan, USA* (JACoW, Geneva, 2015).

[3] R. Takai, H. Enokizono, K. Ito, Y. Mizuno, K. Okabe, and H. Okamoto, Development of a compact plasma trap for experimental beam physics, Jpn. J. Appl. Phys. **45**, 5332 (2006).

[4] H. Okamoto and H. Tanaka, Proposed experiment for the study of beam halo formation, Nucl. Instrum. Methods Phys. Res., Sect. A **437**, 178 (1999).

[5] H. Okamoto, Y. Wada, and R. Takai, Radio-frequency quadrupole trap as a tool for experimental beam physics, Nucl. Instrum. Methods Phys. Res., Sect. A **485**, 244 (2002).

[6] S. Ohtsubo, M. Fujioka, H. Higaki, K. Ito, H. Okamoto, H. Sugimoto, and S. M. Lund, Experimental study of coherent betatron resonances with a Paul trap, Phys. Rev. ST Accel. Beams **13**, 044201 (2010).

[7] H. Takeuchi, K. Fukushima, K. Ito, K. Moriya, H. Okamoto, and H. Sugimoto, Experimental study of resonance crossing with a Paul trap, Phys. Rev. ST Accel. Beams **15**, 074201 (2012).

[8] H. Okamoto, M. Endo, K. Fukushima, H. Higaki, K. Ito, K. Moriya, S. Yamaguchi, and S. M. Lund, Experimental simulation of beam propagation over long path lengths using radio-frequency and magnetic traps, Nucl. Instrum. Methods Phys. Res., Sect. A **733**, 119 (2014).

[9] K. Fukushima, K. Ito, H. Okamoto, S. Yamaguchi, K. Moriya, H. Higaki, T. Okano, and S. M. Lund, Experimental verification of resonance instability bands in quadrupole doublet focusing channels, Nucl. Instrum. Methods Phys. Res., Sect. A **733**, 18 (2014).

[10] K. Moriya, K. Fukushima, K. Ito, T. Okano, H. Okamoto, S. L. Sheehy, D. J. Kelliher, S. Machida, and C. R. Prior, Experimental study of integer resonance crossing in a nonscaling fixed field alternating gradient accelerator with a Paul ion trap, Phys. Rev. ST Accel. Beams **18**, 034001 (2015).

[11] K. Moriya, M. Ota, K. Fukushima, M. Yamaguchi, K. Ito, and H. Okamoto, Double stop-band structure near half-integer tunes in high-intensity rings, Phys. Rev. Accel. Beams **19**, 114201 (2016).

[12] K. Ito, H. Okamoto, Y. Tokashiki, and K. Fukushima, Coherent resonance stop bands in alternating gradient beam transport, Phys. Rev. Accel. Beams **20**, 064201 (2017).

[13] K. Ito, M. Matsuba, and H. Okamoto, Effect of quadrupole focusing-field fluctuation on the transverse stability of intense hadron beams in storage rings, Prog. Theor. Exp. Phys. **2018**, 023G01 (2018).

[14] T. Ikeda, K. Ito, and H. Okamoto, Novel tabletop experiment demonstrating the nonlinear resonance excitation observed at the CERN Proton Synchrotron, Jpn. J. Appl. Phys. **60**, 070901 (2021).

[15] L. Groening, W. Barth, W. Bayer, G. Clemente, L. Dahl, P. Forck, P. Gerhard, I. Hofmann, M. S. Kaiser, M. Maier, S. Mickat, T. Milosic, D. Jeon, and D. Uriot, Experimental Evidence of the 90 Stop Band in the GSI UNILAC, Phys. Rev. Lett. **102**, 234801 (2009).

[16] Accelerator Technical Design Report for High-Intensity Proton Accelerator Facility Project, J-PARC, edited by Y. Yamazaki, Report No. JAERI-Tech 2003-44, KEK Report No. 2002-13, 2003.

[17] P. K. Ghosh, *Ion Traps* (Oxford Science, Oxford, 1995).

[18] H. Okamoto, K. Kojima, and K. Ito, A compact Paul ion trap for the study of space-charge effects in drift-tube linear accelerators, Prog. Theor. Exp. Phys. **2019**, 093G01.

[19] I. M. Kapchinskiy, *Theory of Resonance Linear Accelerators* (Harwood Academic Pub., New York, 1985).

[20] R. D. Ryne, Finding matched rms envelopes in rf linacs: A Hamiltonian approach, Los Alamos Report No. LA-UR-95-391, 1995.

[21] J. Qiang, R. D. Ryne, S. Habib, and V. Decyk, An object-oriented parallel particle-in-cell code for beam dynamics simulation in linear accelerators, J. Comput. Phys. **163**, 434 (2000).

[22] Y. Yamane, H. Okamoto, and K. Kojima, Excitation and suppression of synchrobetatron resonances in high-intensity hadron linacs, Phys. Rev. Accel. Beams **24**, 084201 (2021).

[23] T. P. Wangler, *RF Linear Accelerators* (John Wiley & Sons, New York, 1998).

[24] See the section written by J. Wei in Ref. [26] and references therein.

[25] E. D. Courant and H. S. Snyder, Theory of the alternating-gradient synchrotron, Ann. Phys. (N.Y.) **3**, 1 (1958).

[26] *Handbook of Accelerator Physics and Engineering*, edited by A. W. Chao and M. Tigner (World Scientific, Singapore, 1991).

[27] K. Kojima, M. Goto, H. Higaki, K. Ito, and H. Okamoto, A linear Paul trap without the use of the transverse quadrupole field, Plasma Fusion Res. **17**, 1406003 (2022).

[28] I. Hofmann, L. J. Laslett, L. Smith, and I. Haber, Stability of the Kapchinskij-Vladimirskij (K-V) distribution in long periodic transport systems, Part. Accel. **13**, 145 (1983).

[29] J. Struckmeier and M. Reiser, Theoretical studies of envelope oscillations and instabilities of mismatched intense charged-particle beams in periodic focusing channels, Part. Accel. **14**, 227 (1984).

[30] S. M. Lund and B. Bukh, Stability properties of the transverse envelope equations describing intense ion beam transport, Phys. Rev. ST Accel. Beams **7**, 024801 (2004).

[31] I. Hofmann and O. Boine-Frankenheim, Parametric instabilities in 3D periodically focused beams with space charge, Phys. Rev. Accel. Beams **20**, 014202 (2017).
[32] J. Qiang, Three-dimensional envelope instability in periodic focusing channels, Phys. Rev. Accel. Beams **21**, 034201 (2018).
[33] I. Hofmann, A. Oeftiger, and O. Boine-Frankenheim, Self-consistent long-term dynamics of space charge driven resonances in 2D and 3D, Phys. Rev. Accel. Beams **24**, 024201 (2021).
[34] K. Kojima and H. Okamoto, Characterization of overlapping betatron resonances above the phase advance of 90° per cell, Phys. Rev. Accel. Beams **25**, 024201 (2022).
[35] K. Kojima, H. Okamoto, and Y. Tokashiki, Empirical condition of betatron resonances with space charge, Phys. Rev. Accel. Beams **22**, 074201 (2019).
[36] K. Kojima, H. Okamoto, and Y. Tokashiki, Reply to "Comment on 'Empirical condition of betatron resonances with space charge'", Phys. Rev. Accel. Beams **23**, 028002 (2020).
[37] H. Okamoto, M. Aoki, C. Ichikawa, K. Kojima, T. Kurauchi, and Y. Yamane, Coherent and incoherent space-charge effects in high-intensity hadron rings, J. Instrum. **15**, P07017 (2020).
[38] Note that even a tail particle may have a large incoherent tune shift in a particular direction, depending on its spatial trajectory.
[39] F. J. Sacherer, Ph.D thesis, Lawrence Radiation Laboratory, 1968; Report No. UCRL-18454, 1968.
[40] H. Okamoto and K. Yokoya, Parametric resonances in intense one-dimensional beams propagating through a periodic focusing channel, Nucl. Instrum. Methods Phys. Res., Sect. A **482**, 51 (2002).
[41] I. Hofmann and O. Boine-Frankenheim, Revisiting the Longitudinal 90° Limit in High Intensity Linear Accelerators, Phys. Rev. Lett. **118**, 114803 (2017).
[42] The coherent dipole ($m = 1$) resonance cannot be excited under the lattice condition considered here.
[43] R. A. Jameson, Beam-intensity limitations in linear accelerators, IEEE Trans. Nucl. Sci. **28**, 2408 (1981).
[44] K. Ito, T. Kurauchi, H. Higaki, and H. Okamoto, Experimental observation of low-order collective oscillation modes in a strong-focusing lattice, J. Phys. Conf. Ser. **1350**, 012125 (2019).